

Stationary Internal Cooling Passage Experiments for an Engine Realistic Configuration

J. C. Ryley - M. McGilvray - D. R. H. Gillespie

Osney Thermo-Fluids Lab, University of Oxford, Oxford, UK

ABSTRACT

Stationary experiments were conducted on an engine representative internal cooling passage with a filleted rectangular cross-section with staggered 45° ribs on two opposing walls. The ribs had a rounded profile and span half the width of the passage. Pressure loss measurements and spatially resolved heat transfer coefficients have been collected over the full surface of the test section over a range of Reynolds numbers (18,000 - 105,000) for two aspect ratios, 1:2 and 1:3. The experimental results were compared to widely used empirical correlations for ribbed passages with full width ribs in sharp-cornered passages. The average Nusselt number and friction factor differed to correlations by a maximum of 45% and 10% respectively.

NOMENCLATURE

Symbols		Subscripts	
A	Area	$[m^2]$	0 Reference
c	Direction of curvature		fp flat plate
c_p	Specific heat capacity at constant pressure	$[J/(kg.K)]$	r radial corrected
D_h	Hydraulic diameter	$[m]$	s Surface
e	Rib height	$[m]$	x cross-section
f	Friction factor	$\Delta P \frac{D_h}{2\rho V^2 L}$	Greek
H	Passage height	$[m]$	α Rib angle
h	Heat transfer coefficient	$[W/(m^2.K)]$	β Equation 2
k	Thermal conductivity	$[W/(m.K)]$	μ Viscosity
Nu	Nusselt number	$\frac{hD_h}{k}$	ρ Density
Pr	Prandtl number (0.71)	$\frac{c_p \mu}{k}$	σ Solution index
p	Rib pitch	$[m]$	Abbreviations
P	Perimeter	$[m]$	AR Aspect Ratio (W/H)
r	Radius	$[m]$	HTC Heat Transfer Coefficient
Re	Reynolds number	$\frac{\rho v D_h}{\mu}$	LE Leading Edge
T	Temperature	$[K]$	PS Pressure Side
t	Time	$[s]$	SS Suction Side
v	Velocity	$[m/s]$	TE Trailing Edge
W	Passage width	$[m]$	THTAC Transient Heat Transfer Analysis Code

INTRODUCTION

The continued drive to increase engine efficiency, in order to lower fuel consumption and environmental impact, has led to a rise in the turbine entry temperature. Raising this further is constrained by HP turbine blade and vane material temperatures, where a 10-15K rise in component temperature may reduce blade life by half (Alfaro-Ayala et al., 2011). Improvements in the design of HP turbine blade internal cooling system, whilst maintaining component life, would allow for an increase in gas temperature and/or a reduction in coolant mass flow rate; ultimately both result in a reduction of specific fuel consumption.

Existing technology used in mid-section internal cooling passages is primarily based around rib turbulators. This allows long passages to be employed which exploit the full temperature potential of the coolant, prior to ejection as a coolant film. There is a large collection of research in this field investigating how various geometric factors influence heat transfer and pressure drop, notably by Han et al. (2000). Data from studies have been collated in empirical formulas and are used in developing designs of internal cooling passages, a common industry practice (Walker and Zausner, 2007).

Numerical simulations (CFD) are commonly used to investigate component design, and are compared to existing experimental data for validation. Many different methodologies are employed for such comparisons (Walker and Zausner, 2007; Hagari et al., 2011; Shevchuk et al., 2008). In the open literature there is no comparison that demonstrates which method is most effective. The majority of the methods compare bulk heat transfer coefficient (HTC) values and, in doing so, fail to evaluate whether detailed features are captured. This limitation is highlighted in numerical optimisation schemes, which given a set of constraints, look for a design with the best performance. This requires that the heat transfer distributions in the passage are accurately modelled. If numerical results are validated only against an area averaged value, without considering the accuracy of the trends in heat transfer, this could potentially lead to false results when optimising.

Experimental investigations conducted in this field have tended to focus on highly idealised geometries, with sharp edged ribs and passages. A more engine representative passage may contain additional features, such as: filleted ribs, which may not extend across the full width of the passage, a non-rectangular and/or variable passage cross-section, and the presence of film-cooling bleed holes. Schüler et al. (2009) highlighted the need for investigations into engine representative geometries, in order to capture flow pattern characteristics, whilst remaining sufficiently generic to allow wide application of the results. Rallabandi et al. (2011) experimentally investigated the difference caused by rounded rib profiles by comparing results to the sharp edged correlation of Han et al. (1989). This demonstrated a significant change in the friction factor and Nusselt number (respective values from the Rallabandi correlation are up to 19% and 29% greater, at the conditions of the current research) and provided empirical correlations. A direct recommendation from the authors was for further work to obtain locally resolved HTC. Jackson et al. (2009) presented a comparison of numerical and experimental studies on a highly representative model of a multi-pass internal cooling passage. Although this was a highly complex study, only qualitative judgements can be made due to the results being normalised using an unknown method. Also, there is a lack of experimental resolution and measurements were only made on ribbed surfaces. The numerical simulations under-predicted the experimental HTC values on the ribbed wall by up to 20% for the average values, and up to 25% for peak values.

The rotation of the passage has a significant impact upon heat transfer (Huh et al., 2011) through buoyancy and Coriolis forces. Correlations exist to account for the shift in heat transfer for ribbed walls, based on experiments taking bulk heat transfer measurements. Due to the complex nature of rotating experiments it is very challenging to obtain spatially resolved values for heat transfer. By conducting high spatial resolution experiments under stationary conditions and low resolution rotational experiments, CFD studies can be validated and further numerical studies undertaken to analyse the effect of rotation.

This paper presents results from stationary experiments of a generic engine representative internal cooling passage, over a range of Reynolds numbers at two aspect ratios. Transient liquid crystal techniques developed by Ireland and Jones (2000) and Wang et al. (1991) have been implemented to collect HTC over the full surface of the passage and provide bulk HTC on the ribs. Corresponding measurements of pressure drop in the passage were also recorded. Investigations have been conducted into how results differ from those collected in previous studies on more idealised geometry.

EXPERIMENTAL SET UP

Experimental facility

A summary of the experimental setup is provided below. Figure 1 presents a schematic of the stationary internal cooling rig, which includes a single pass of a rib turbulated passage. The rig is operated in a suction mode, with the outlet plenum connected to a vacuum line, which contains a gate valve in order to set the mass flow rate through the system. A flow straightener and baffle plate are located before and after the test section respectively in order to promote flow uniformity through the passage. A heater mesh is situated 400 mm upstream of the intake to the test section to provide a rapid change in temperature used in the transient liquid crystal technique. Five K-type gas thermocouple measurements along the centreline, and five static pressure measurements (using multiple pressure transducers, Sensortech HX and BTE range) are recorded over the length of the test section, on the trailing edge surface 10 mm from the centreline. The pressure gradient used to calculate the friction was measured over the range $5 < x/D_h < 15$. This compares to $4 < x/D_h < 14$ in the studies of Rallabandi et al. (2011). Data is logged using a National Instruments data acquisition system (SCXI-1000 chassis containing a SCXI-1102 card) driven by Labview software.

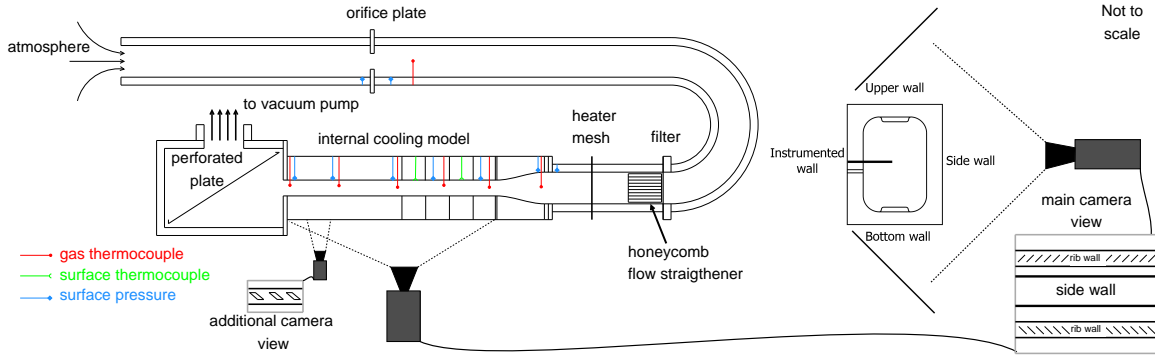


Figure 1: Schematic of experimental setup of flow path, instrumentation and camera view.

Mirrors are placed above and below the test section at an angle of 45° , to allow the main camera to capture three of the surfaces during a single test. A second camera views a short section of the downstream ribbed wall to capture high spatial resolution data. An LED is present in both cameras' fields of view and is activated when power is supplied to the heater mesh. This provides synchronisation between the video and logged temperature data. The surface is lit by four 'warm white' LED strip lights directed at the test section to provide the best illumination with minimal reflections.

The test section is constructed from Perspex (thermal product $569 \pm 29 \frac{W}{m^2 s^{0.5} K^1}$ (Ireland, 1987)), which is a good thermal insulator and provides optical access. The internal surface of the test section is coated with a mixture of a binder and three narrow band liquid crystals ($1^\circ C$ activation, nominally 25, 30, and $35^\circ C$). A black ink backing is applied to provide better contrast.

The material thickness would allow the assumption of a 1-D semi-infinite wall to remain valid during a 75 s test duration for the case of uniform HTC over the surface (Shultz and Jones, 1973). In the current study strong gradients in HTC are expected. Ling et al. (2003), amongst other workers have shown that lateral conduction may be considered insignificant when:

$$\frac{d^2 q}{dx^2} \ll \frac{q}{2\alpha t} \quad \text{and} \quad \frac{d^2 q}{dy^2} \ll \frac{q}{2\alpha t} \quad (1)$$

The high curvature and extremely high HTC gradients expected on the ribs meant that the 1-D conduction equation would clearly be invalid and an alternative approach required. On the plane surface surrounding the ribs, by limiting the test time to 30 s, the criteria above could be largely satisfied in spite of large changes in HTC. A hybrid technique allows bulk values of HTC to be calculated over the ribs (Wang et al., 1991). To use this technique several of the Perspex ribs were replaced with brass inserts. This technique uses a lumped heat capacity model with temperature

measured at the Perspex interface, as the inserts have a low Biot number. The brass inserts were backed with the same liquid crystal mixture used on the passage walls to measure temperature and affixed to the Perspex with the binder.

During a test, the model is initially at an isothermal temperature to the surroundings. Air from the atmosphere is then passed, unheated, through the rig and the mass flow rate is adjusted to obtain the desired Reynolds number. The test is initiated when power is supplied to the heater mesh. Calibration of all liquid crystals was performed in-situ: the liquid crystal colour play adjacent to a surface thermocouple is recorded as the surface temperature is increased over a fine series of steady state temperatures covering the full colour play range of the liquid crystals. In-situ calibration removes distortion effects caused by lighting or the local white balance of the cameras. Separate calibrations are required for the perspex surfaces and hybrid ribs.

Passage Geometry

The internal cooling passage test section consists of a 432 mm long rounded rectangular duct with rib turbulators on two opposing walls (suction and pressure surface), the remaining walls (leading and trailing edge) are smooth, as seen in Figures 2 and 3. Ribs in the passage are at an angle (α) of 45° to the streamwise direction; a pitch to height spacing (P/e) of 10; filleted along all edges (radius of filleting is $e/2$); centred in the passage; span half the width of the passage; staggered by half the pitch between the suction and pressure surface. Two different aspect ratios (width:height) of 1:2 and 1:3 were investigated, with rib blockage (e/D_h) of 6.9% and 6.2% and a hydraulic diameter of 26.1 and 29.0 mm respectively. The passage width (W) is 18.66 mm. The rig can be reconfigured, so that the instrumentation is on the opposite planar wall, to allow HTC data to be collected for the 4th wall.

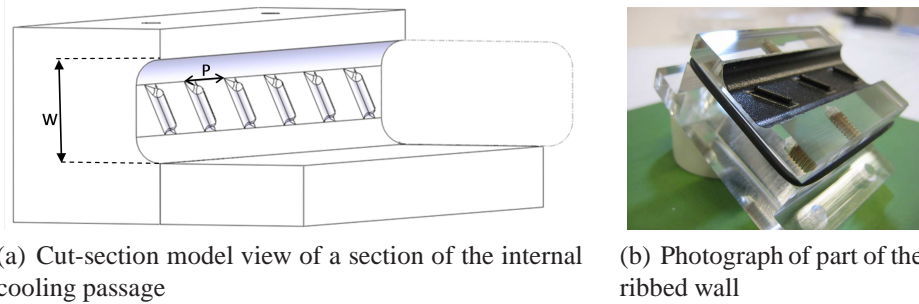


Figure 2: **Schematic and image of rib turbulators in experimental passage.**

HTC DATA ANALYSIS

Post-processing involves transforming the recorded experimental data of gas temperatures and video into a heat transfer coefficient contour map of the unwrapped inner surface of the internal cooling passage. The recorded video is cropped to only the surfaces of interest, and a third order power correction for barrel lens effect is applied.

The transient liquid crystal technique provides a nearest match for the HTC value at each pixel location. By modelling the gas temperature as a series of ramps (Ireland and Jones, 2000) surface temperature can be calculated for a given HTC value using the semi-infinite 1D conduction equation (Equation 2). A theoretical green intensity history can then be produced using calibration data. By generating a series of theoretical green intensity profiles at each pixel over a range of HTC values and the recorded driving gas temperature. A nearest value of HTC can then be evaluated by finding the value of HTC which produces the minimum RSS difference between the recorded and theoretical intensity profiles. In this work the centreline gas temperature is used to calculate the HTC, the gas temperature is linearly interpolated between the thermocouples for each pixel.

$$T_s = T_0 + \sum_{i=1}^n m_i t \left(1 - \frac{2}{\beta_i \sqrt{\pi}} + \frac{1 - \exp(\beta_i^2) \operatorname{erfc}(\beta_i)}{\beta_i^2} \right), \quad \beta_i = \frac{h(t - t_i)^{\frac{1}{2}}}{\sqrt{\rho c k}}, \quad m_i = \frac{(\Delta T_{gas, \infty})_i}{\Delta t} \quad (2)$$

The hybrid rib method operates in the same manner using adjusted versions of the appropriate equations (Wang et al., 1991) for pixels located on ribs. After the HTC is calculated for each pixel on a given rib, any outliers are rejected then the median is taken as the rib's HTC level.

Recombination and transformation to spatial dimensions

The data from each surface are transformed, using a linear interpolation to account for non-linearity in radial geometry and rotation, and combined to form a single map, as shown in Figure 3. Where there is an overlap between images the data are cropped to the midpoint of the passage fillet for recombination. This minimises the area scaling applied to individual pixels. Each wall is appropriately rotated to reflect the layout of the experimental passage. To account for radial conduction in the concave corners, the curvature correction method of Buttsworth and Jones (1997) is applied, Equation 3, to values determined assuming a planar surface.

$$h_r = h_{fp} - \frac{ck}{2r} \quad (3)$$

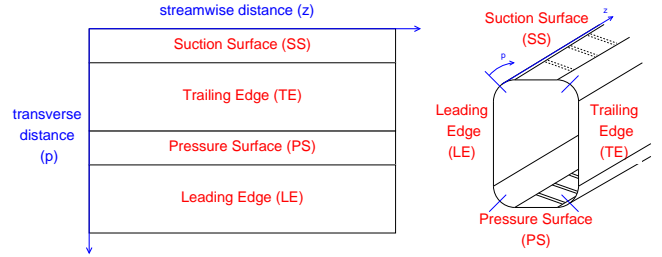


Figure 3: **Schematic for recombination of HTC maps from each individual wall into a unitary map.**

Uncertainty Analysis

A perturbation method (Kline and McClintock, 1953) has been applied to calculate the uncertainty in experimental measurements, assuming all experimental uncertainties are independent. Using the uncertainty of each measurement, a maximum uncertainty has been assessed at each pixel location and presented in the form of contour maps. An example is given in Figure 4. The following experimental uncertainties were applied based on both the measurement uncertainty and experimental fluctuation/non-uniformity: time 0.033 s (0.04 s for the secondary camera); liquid crystal calibration 0.5%, initial temperature 0.5%, gas temperature 0.5% all as temperature in °C; Perspex thermal product 5.1%. For the hybrid ribs: density 0.5%; specific heat capacity 5%; thermal conductivity 5%. Mass flow rate measurements are calculated to have an uncertainty of less than 1.3% and friction factor typically less than 2%.

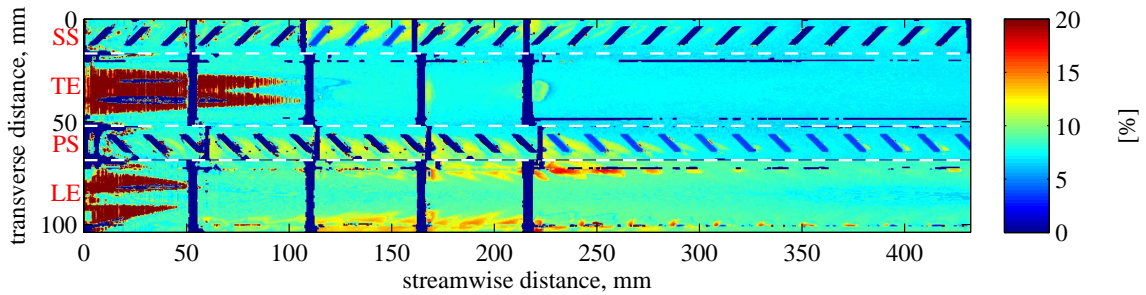


Figure 4: **Combined total uncertainty in HTC map for a Reynolds number of 60596, AR 1:2.**

The HTC uncertainty typically ranges from 6-18%, depending on the geometric and flow features in the region, for the Perspex test section and is 6% for the hybrid ribs. The uncertainty for the higher resolution images is up to 10% lower than the main camera, showing that resolution has a significant impact on the uncertainty. Repeat experiments for both aspect ratios showed agreement within 10%, which is lower than the maximum calculated value of 18%, though similar to the average value of under 10%. By applying the empirical correlations of (Han et al., 1989), the mass flow rate uncertainty relates to spatially averaged uncertainty in HTC of $\leq 2\%$.

Correlations and data normalisation

Experimental results are compared to correlations from the literature whose applicability is dependent on experimental passage geometry. The correlation of Han et al. (1989) is for an sharp cornered passage with full width sharp-edged ribs. The correlation of Rallabandi et al. (2011) is for the same geometry but with filleted ribs with radii of half the rib height ($e/2$). Both correlations are for the ribbed surfaces only. Thus, the pressure/suction surfaces are only compared to the correlations. Nusselt number and friction factor data are normalised by the Dittus-Boelter and Blasius relations for turbulent, fully developed smooth pipe flow (Equation 4). Experimental averages are taken over the downstream half (216 - 432 mm) of the passage, where the flow is more developed and bulk HTC values have been calculated for the ribs.

$$\text{Nu}_0 = 0.023\text{Re}_{D_h}^{0.8}\text{Pr}^{0.4}, \quad f_0 = 0.079\text{Re}_{D_h}^{-0.25} \quad (4)$$

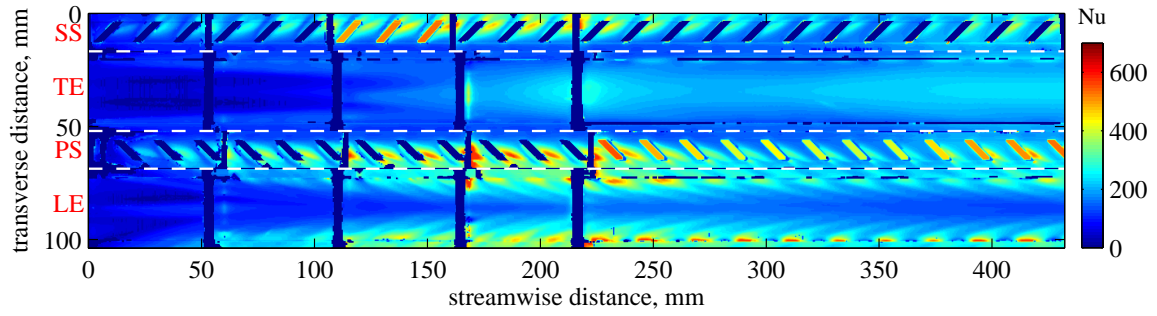
Comparison of results to empirical correlations, although useful, is acknowledged to have its limitations. Firstly, the present experimental data may not be fully developed over the region where average data is taken. Additionally, the experimental data on which the Rallabandi et al. (2011) correlation is formulated has streamwise variations in normalised Nusselt number of up to $\sim 25\%$ over the region where the flow is assumed to be fully developed. Secondly, the present experimental HTC values are based on interpolated centreline temperature and not mixed bulk temperatures used in the correlations, which can lead to significant discrepancies as shown in the associated numerical simulations (McGilvray et al., 2013). However, the Rallabandi et al. (2011) HTC data is calculated from a single point measurement of the temperature. Finally, the present geometry is slightly outside the range tested in creating both correlations. However, this effect may be minimal due to a large spread of e/D_h values (9.4-18.8%) used in its development and with knowledge that the Han et al. (1989) correlation has been verified by experimental data for lower e/D_h configurations.

RESULTS

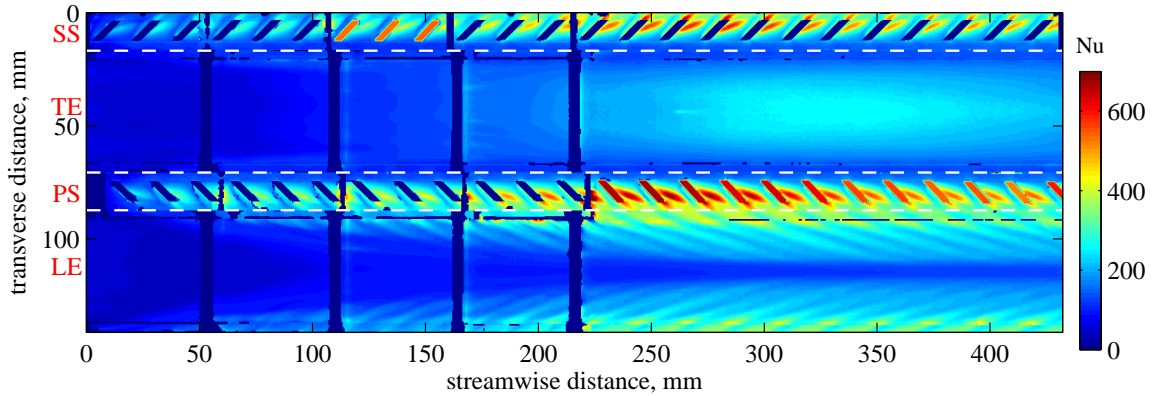
Heat transfer coefficients have been collected over the full internal surface of two aspect ratio configurations at five Reynolds numbers (18,000-105,000). Streamwise static pressure measurements were taken over a finer range of Reynolds numbers to evaluate the frictional losses in both cases. Heat transfer results are presented in terms of Nusselt number, based on the hydraulic diameter and the average air temperature over the test period at each pixel location. Prandtl number was taken as 0.71. Where there are corrupt data (such as at joints in the model) these are set as NaN in averaging procedures, but displayed as zero values in contour plots. On the Perspex ribs, accurate values can not be calculated as a 3-D conduction correction is required: these are also set as NaN.

Figure 5 presents examples of the spatially resolved Nusselt number data on the internal surface of each passage. These maps demonstrate the typical heat transfer patterns observed for both aspect ratios and all Reynolds numbers. The Nusselt number is low on the side walls at the entrance to the passage, as it is fed from a region of developed flow upstream. On both the pressure and suction side ribbed walls, the levels are generally higher. High heat transfer is observed in the reattachment regions between each rib, and behind of the downstream edge of each rib. The Nusselt number is higher on the leading edge side of the ribbed walls compared to the trailing edge side; streaks of high Nusselt number on the leading edge wall are from the secondary flow washing up from the inter-rib regions. A region of lower Nusselt number runs along the centre of the wall which is lower than average level on the opposing trailing edge wall and is associated with secondary flow detachment. In contrast, variation in Nusselt number across the trailing edge is low, with values slightly higher near the centre.

Figure 6, presents the same experimental results as Figure 5 averaged around the perimeter, and broken down into different regions to highlights trends and contributions to Nusselt number down the passage. Normalising the data allows for improvement over a smooth walled passage to be observed.



(a) Nusselt number maps for a Reynolds number = 60596 at an aspect ratio of 1:2.



(b) Nusselt number maps for a Reynolds number = 59409 at an aspect ratio of 1:3.

Figure 5: Nusselt number distributions for both aspect ratios at a Reynolds number of 60,000.

Spikes and dips seen in the data correspond to joints (restricted views and slight misalignments). Values for ribs are only available where hybrid ribs are present. For both aspect ratios, the ribs have 1.5-2 times larger heat transfer than the inter-rib averages. This is partly due to the data being presented based on projected area: if based on surface area, a 33% decrease in average Nusselt number would be expected on the ribs. The flow does not fully develop (i.e. plateau with streamwise distance) for either aspect ratios and at all Reynolds numbers investigated.

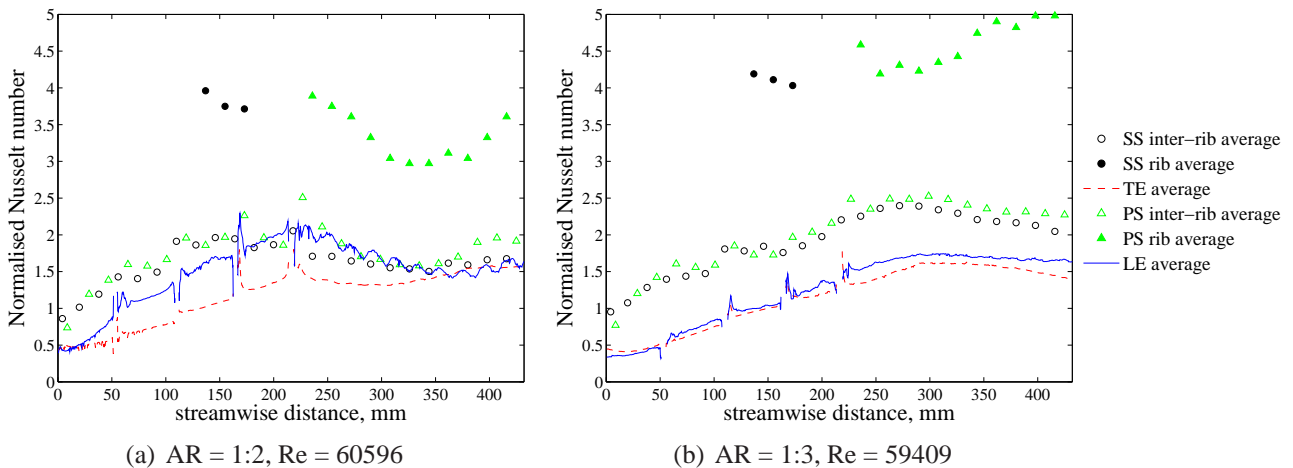


Figure 6: Average normalised Nusselt number streamwise distributions for both aspect ratios at a Reynolds number of 60,000.

Comparing the two aspect ratios, the pattern of Nusselt number is generally very similar in terms of the overall features. Both the trailing and leading edges have similar levels, however, the secondary flow appears to extend across the entire leading edge in the case of the 1:2 aspect ratio. A noted difference is a peak in average Nusselt number, located close to 220 mm and again near 400 mm

for the 1:2 aspect ratio, and further downstream at ~ 275 mm when moving to the 1:3 aspect ratio. Additionally, the Nusselt number on the ribs and in the post rib reattachment regions is higher for the 1:3 aspect ratio configuration.

Figure 7 presents the projected area averaged Nusselt number for the downstream half of the passage, and empirical correlations for the ribbed wall. It clearly shows the impact of Reynolds number on average Nusselt number and that engine realistic features impact heat transfer levels compared to idealised geometry. For the 1:2 aspect ratio configuration, the average Nusselt number is consistently lower than the correlations and the deviation is seen to increase with Reynolds number. In contrast, the pressure surface average for the 1:3 aspect ratio results continues to increase above the correlation as Reynolds number rises. As Reynolds number increases, the leading edge average value is seen to tend towards the ribbed wall average, whilst the trailing edge average falls relative to the total passage average, reflecting stronger secondary flow. Using the total average Nusselt numbers for the AR 1:2 and 1:3, power laws were developed as presented in Equations 5 and 6 respectively.

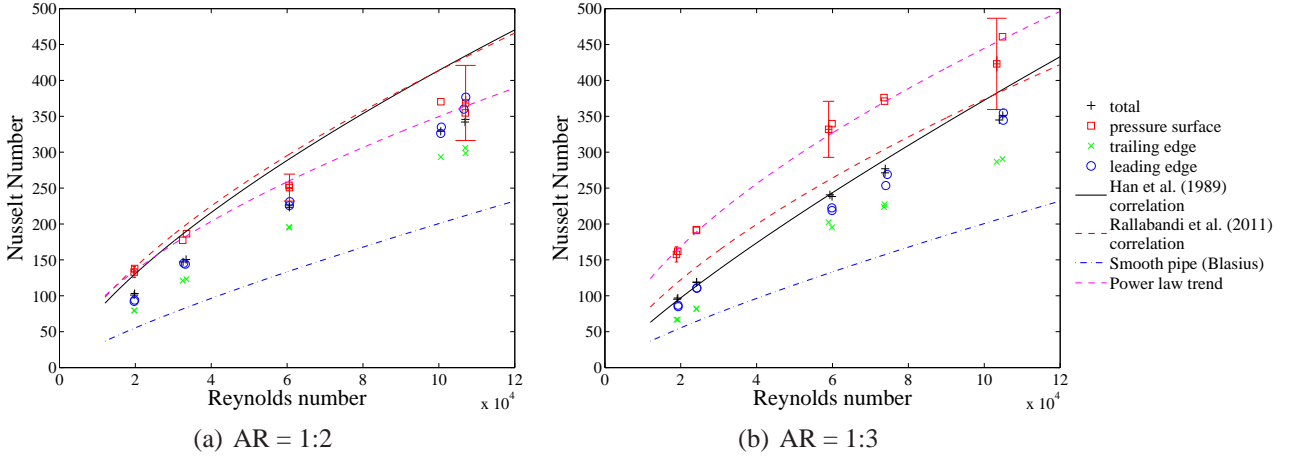


Figure 7: **Projected area averaged Nusselt number as a function of Reynolds number compared to correlations for the ribbed wall. Averages are taken over the downstream (216-432 mm) half of the passage. Uncertainty bars shown for three Reynolds numbers.**

$$Nu_{1:2} = 0.041Re_{D_h}^{0.7855} \quad (5)$$

$$Nu_{1:3} = 0.0595Re_{D_h}^{0.7458} \quad (6)$$

High resolution data (Figure 8) highlights heat transfer shifts towards the leading edge and is reduced (compared to the rib value) on the trailing edge side of the ribbed wall with increasing Reynolds number. As the vortical flow features strengthen (with Reynolds number), the level of Nusselt number in the reattachment region lessens in comparison to the ribs. In the 1:3 passage, the reattachment region has a comparable heat transfer to the rib. In contrast, the higher axial velocity in the AR 1:2 passage appears to weaken this feature. The high resolution maps agree well with the full surface map: typically within 6% on the planar sections. The increased resolution reveals greater subtleties of the heat transfer especially where the secondary flow washes up onto the leading edge wall. Due to the small size and high gradient of some of these features, local discrepancies between the high and low resolution images can be up to 20%, although changes in the averaged values are minimal.

Caution must be applied when drawing conclusions from the data presented. A fair comparison of performance may be made by plotting the total heat transferred per unit volume, $h \cdot A_{surface} / A_x \cdot L$, versus the mass flow rate per unit cross-sectional area for the two passages, Figure 9. While the data nearly collapses to a single trend for each surface the 1:2 passage appears to out perform the 1:3 passage for this measure. This is opposite to the Nusselt number to Reynolds number relationship which is shown in Figure 7

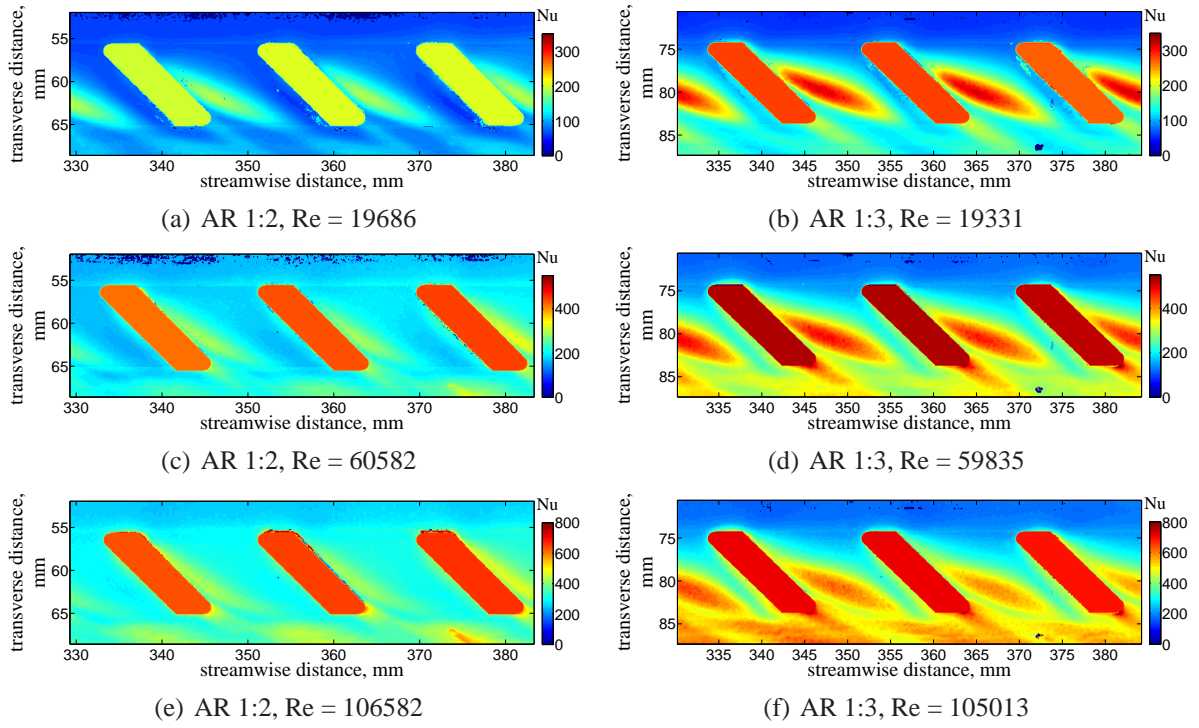


Figure 8: Nusselt number distributions of the pressure side walls between the 1:2 and 1:3 aspect ratios at similar Reynolds numbers. Rib values are bulk values based on projected area.

Figure 10 compares the experimental normalised friction factor the empirical correlations. As previously discussed in this paper the correlations have been developed for a different geometry and flow development. As expected the friction factor results are not seen to completely agree with either of the correlations, although the difference in the friction factors between the two aspect ratios is noted to be similar.

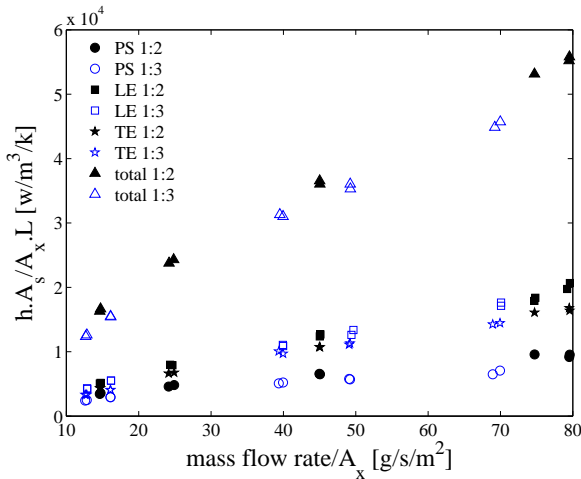


Figure 9: Average Nusselt number on downstream half of total passage. Scaled to $T_{gas} = 45^\circ\text{C}$. Passage width fixed, $w = 18.66\text{mm}$.

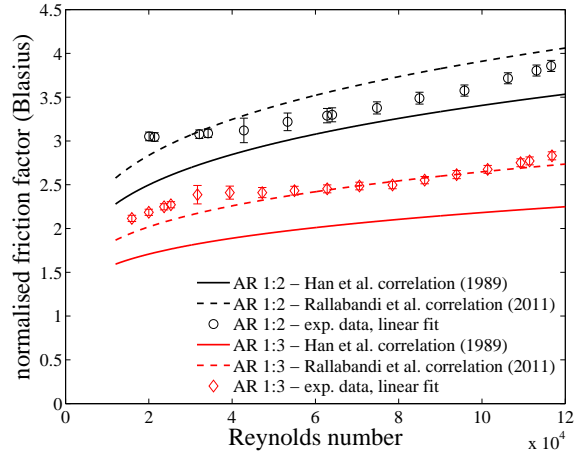


Figure 10: Normalised friction factor as a function of Reynolds number for both aspect ratio configurations.

SUMMARY AND CONCLUSIONS

Heat transfer and pressure loss measurements have been made in a stationary engine representative internal cooling passage. Spatially resolved heat transfer data and corresponding uncertainties were obtained over the full surface of the test section. With the use of a hybrid rib technique, bulk values of HTC have been presented on the rib turbulators. The overall profile of heat transfer was similar for both aspect ratios at all Reynolds numbers, though local behaviour especially around ribs

changed significantly. With increasing Reynolds number, spatial gradients of Nusselt number were seen to decrease. Suitably averaged values provide a method of direct comparison between different geometric data sets and allow comparison to other studies. The spatially resolved distributions over the full surface provides a greater understanding of the heat transfer structures allowing validation of CFD studies, and diagnosis of areas in which modelling is insufficient. With the use of numerical tools, additional drivers of heat transfer such as rotation and film cooling bleed holes can be added with knowledge of the accuracy of the stationary passage heat transfer.

ACKNOWLEDGEMENTS

This research received funding from the European Union Seventh Framework Programme (FP7/2007-2013) under grant agreement no. 233799 (ERICKA). The authors acknowledge the contributions to this work from Trevor Godfrey, Gerald Walker, Dave Mountain and EDM.

REFERENCES

- Alfaro-Ayala, J., Gallegos-Muñoz, A., Riesco-Avilla, J., Flores-López, M., Campos-Amezcuca, A., and Mani-González, A. (2011). Analysis of the flow in the combustion - transition piece considering the variation in the fuel composition. *Journal of Thermal Science and Engineering Applications*, 3.
- Buttsworth, D. R. and Jones, T. V. (1997). Technical note: Radial conduction effects in transient heat transfer experiments. *Aeronautical Journal*, 101(1005):209–212.
- Hagari, T., Ishida, K., Oda, T., Douura, Y., and Kinoshita, Y. (2011). Heat transfer and pressure losses of w-shaped small ribs at high reynolds numbers for combustor liner. *Journal of Engineering for Gas Turbines and Power*, 133.
- Han, J., Dutta, S., and Ekkad, S. (2000). *Gas Turbine Heat Trasfer and Cooling Technology*. Taylor and Francis. ISBN: 15603284.
- Han, J., Ou, S., Park, J., and Lei, C. (1989). Augmented heat transfer in rectangular channels of narrow aspect ratios with rib turbulators. *International Journal of Heat and Mass Transfer*, 32(9):1619–1630.
- Huh, M., Liu, Y., liu, Y., and Han, J. (2011). High rotation number effect on heat transfer in a rectangular (AR=2:1) two-pass channel. *ASME Journal of Heat Transfer*, 133.
- Ireland, P. (1987). Internal cooling of turbine blades. D.phil thesis, University of Oxford.
- Ireland, P. T. and Jones, T. V. (2000). Liquid crystal measurements of heat transfer and surface shear stress. *Measurement Science Technology*, pages 969–986.
- Jackson, D., Ireland, P., and Cheong, B. (2009). Combined experimental and CFD study of HP blade multi-pass cooling system. *Proceedings of ASME Turbo Expo 2009; Power for Land, Sea and Air*, (GT2009-60070).
- Kline, S. and McClintock, F. A. (1953). Describing uncertainties in single-sample experiments. *Mech. Eng.*, page 3.
- Ling, J. P., Ireland, P. T., and Turner, L. (2003). A Technique for processing transient heat transfer, liquid crystal experiment in the presence of lateral conduction. Technical Report GT2003-38446, Proceedings of ASME Turbo Expo 2003; Power for Land, Sea and Air.
- McGilvray, M. and Gillespie, D. R. H. (2011). THTAC: Transient Heat Transfer Analysis Code. Technical report, Department of Engineering Science, University of Oxford, Great Britain.
- McGilvray, M., Orozco Pieiro, C., Axe, T., Ryley, J., and Gillespie, D. (2013). Comparison of stationary internal cooling passage experimental data to numerical simulations. *10th European Conference on Turbomachinery, Fluid Dynamics and Thermodynamics*.
- Rallabandi, A. P., Alkhamis, N., and Han, J. (2011). Heat transfer and pressure drop measurements for a square channel with 45 deg round-edged ribs at high reynolds numbers. *Journal of Turbomachinery*, 133.
- Schüler, M., Neumann, S. O., and Weigand, B. (2009). Pressure loss and heat transfer in a 180 deg bend of a ribbed two-pass internal cooling channel with engine-simular cross sections, part 1: Experimental investigations. *8th European Conference on Turbomachinery, Fluid Dynamics and Thermodynamics*, (ETC8-115).
- Shevchuk, I., Jenkins, S., Weigand, B., von Wolfersdorf, J., Neumann, S., and Schnieder, M. (2008). Validation and analysis of numerical results for a varying aspect ratio two-pass internal cooling channel. *Proceedings of ASME Turbo Expo 2008; Power for Land, Sea and Air*, (GT2008-51219).
- Shultz, D. and Jones, T. (1973). Heat transfer measurements in short-duration hypersonic test facilities. AGARDograph 165, Department of Engineering Science, University of Oxford, Great Britain.
- Walker, D. and Zausner, J. (2007). RANS evaluation of internal cooling passage geometries: Ribbed passages and a 180 degree bend. *Proceedings of ASME Turbo Expo 2007; Power for Land, Sea and Air*, (GT2007-278).
- Wang, Z., Ireland, P., and Jones, T. (1991). A technique for measuring convective heat transfer at rough surfaces. *Transactions of the Institute of Measurement and Control*, 13(3):145–154.